

Electric transport in organic system with planar DBP/F₁₆ZnPc junction on the basis of direct current and small signal admittance spectra analysis

Rafał Marczyński, Justyna Szostak, Ryszard Signerski, Grażyna Jarosz*

Faculty of Applied Physics and Mathematics, Gdansk University of Technology, ul. G. Narutowicza 11/12, 80-233 Gdańsk, Poland

Abstract

The objective of this work was to determine electric transport in the organic device based on a planar junction of electron donor and electron acceptor materials, namely ITO/MoO₃/DBP/F₁₆ZnPc/BCP/Ag. The analysis reported herein was based on direct current-voltage measurements and small-signal admittance spectra in the dark and under illumination. Such analysis may provide information on potential barriers, parasitic resistances and presence of space charge affecting the electric current flow within the device. Therefore, this approach could be applied for determination of physical processes related to electric charge transport within multilayer structures, such as photovoltaic cells or photodetectors.

In the case of the investigated system, the parallel parasitic resistance, the resistance of electrodes, and the geometric capacitance of 10 MΩ, 55 Ω, and 1.6 nF respectively were found. It was also shown that the direct current flowing from ITO to Ag was limited by charge carrier injection from electrodes, while in the case of current flowing from Ag to ITO no essential barriers at electrodes were noticed.

Keywords: Organic planar heterojunction, Small signal admittance spectra, Charge transport, Photovoltaic effect

1. Introduction

Solid photovoltaic systems operating on the basis of charge carrier separation at a single heterojunction can be generally divided into inorganic and organic semiconductor devices. Operation principles of inorganic solar cells are well known and efficiencies of particular processes occurring in these systems, starting from absorption of photons and ending with charge carrier collection by electrodes, can be estimated quite accurately. The resultant total efficiencies evaluated from efficiencies of particular processes are in agreement with experiments and the most effective inorganic systems [1] have almost reached the efficiency limit predicted by Shockley-Queisser theory [2]. In the case of organic devices, the most effective systems reach power conversion efficiencies 3 times lower than their inorganic counterparts [1] and processes involved in energy conversion do not seem to be well described. In particular, electric properties of organic junctions raise many doubts. First of all, it is hard to confirm or to rule out the development of space charge region near the junction. Moreover, if it does occur, we can put the question if the width of the region is modified by external electric field, and eventually, if this region provides proper conditions for charge separation. These issues are important for the operation of the device in the dark as well as under illumination.

In this work we analyse electric transport in a planar bilayer organic device in the dark and under illumination with light from the spectral range of strong absorption of both active materials. Our analysis is based on direct current-voltage characteristics and small signal admittance spectra obtained within the 50 Hz - 1 MHz frequency range. Our reasoning regards simultaneous analysis of both components of complex admittance and their relation to direct current-voltage curves collected in the dark and under illumination. Although there are many articles that present the analysis of small signal admittance of organic devices, such an analysis is usually carried out under the assumption of a certain process

*Corresponding author
E-mail address: grajaros@pg.edu.pl (G. Jarosz).

determining these spectra. As a result, these studies are often limited to consideration of only one component of small signal admittance spectra. Assuming the presence of a depletion region near the interface one may determine the width and capacity of this region, distribution of trapping states or the height of a potential barrier on the basis of Mott-Schottky plots (e.g. [3]). Capacity of such a depletion region should be independent of frequency and drop with the increase in reverse voltage. Another example of the analysis regarding only one component of small signal spectra is the analysis of susceptance used to determine mobility of free charge carriers whenever space charge limited current flows through the investigated system. In this case we observe a modulation of the spectrum related to the time of flight of free charge carriers. This method attracts considerable attention since it enables determination of relatively low free charge carrier mobilities in thin organic layers (e.g [4,5]). Another common example of small signal admittance analysis reported in literature is representation of the data in the form of Cole-Cole type of graphs, usually as the negative reactance ($-Z''$) vs resistance (Z') (e.g [6]). This approach enables determination of elements of the equivalent circuit, namely the number of capacitors and resistors necessary to model the device under study. Although it is possible to evaluate the values of resistance, one cannot easily determine the values of capacity on the basis of such plots. The latter are useful whenever changes in the values of chosen elements induced by external factors are the matter of interest (e.g [7,8]). Nevertheless, to assess the values of all the elements the equivalent circuit is comprised of one has to consider both components of frequency dependent small signal admittance. Moreover, knowledge on the effect of DC voltage on small signal spectra is useful for attribution of these elements to geometrical elements of studied system, such as resistance of electrodes or geometrical capacity of the layers, and determination of processes related to charge transport. The correlation between low frequency conductance and current-voltage dependence, as well as the influence of illumination on small signal spectra are also worth studying. There are not many papers showing the analysis of both components of small signal admittance spectra collected for photovoltaic cells under different DC biases. Furthermore, the number of publications dealing with such spectra measured under illumination and referring them to current-voltage characteristics is very limited. Herein, we present a complete analysis of admittance spectra collected for our samples in the dark and under illumination, relating these results to data acquired during DC experiments, and show the application of this approach in the analysis of processes determining electric charge transport in similar systems.

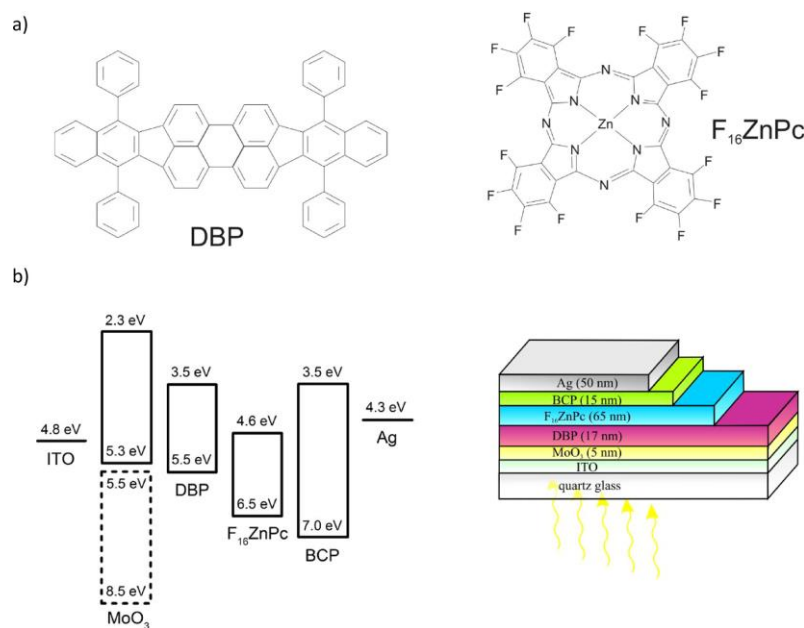


Fig. 1. Chemical structure of DBP on the left and F₁₆ZnPc on the right (a). Energy levels of particular layers of our system on the left and the architecture of the investigated photovoltaic device on the right (b). Energy diagram was drawn on the basis of data presented in [12,21,22] for ITO, in [6,11,19] for MoO₃, [10,11,12] for DBP, [13,23] for F₁₆ZnPc, [13,16,17,24,25] for BCP, [26] for Ag.

The system under study was the ITO/MoO₃/DBP/F₁₆ZnPc/BCP/Ag cell, where ITO is indium tin oxide, MoO₃ is molybdenum trioxide, DBP is tetraphenyldibenzoperiflanthene, F₁₆ZnPc is perfluorinated zinc phthalocyanine and BCP is bathocuproine. DBP was applied as an electron donor [9,10] due to high absorption coefficients of this material reaching over $4 \times 10^5 \text{ cm}^{-1}$ [10–12], while F₁₆ZnPc as an electron acceptor [13,14] that absorbs light of longer wavelengths compared to DBP. Both of these materials form homogeneous layers upon thermal evaporation [12,13]. Complementarity of their absorption spectra should enable harvesting of light from the whole visible range, while the energetic offset between the donor and acceptor layers, shown in Fig. 1, confirms proper conditions for exciton dissociation at the DBP/F₁₆ZnPc junction. We suppose that excitons with energies higher than the difference between LUMO of F₁₆ZnPc and HOMO of DBP can effectively dissociate at the DBP/F₁₆ZnPc interface and as a result of this process electrons populate F₁₆ZnPc, while holes populate DBP. Thin layer of MoO₃ was incorporated into the cell to prevent exciton quenching at the ITO electrode and to enable better hole extraction from DBP to ITO [9,15], while BCP played two roles, namely reduction of exciton quenching at Ag [9,10,13,16,17] and protection of F₁₆ZnPc layer from penetration of Ag atoms during evaporation of the latter. We have to add here, that it is known that vacuum evaporation of MoO₃ does not lead to pure MoO₃ layer but rather to the growth of a MoO_x film [18,19]. Although there are two different views on the energetic structure of such films and mechanisms of electric conduction within these layers (see Fig. 1a), applicability of MoO₃ as a buffer layer has been confirmed by many experiments [9,15,6,20].

2. Experimental

Samples were fabricated under high vacuum of 5×10^{-6} hPa (Auto 306 Turbo, Edwards). Substrates were neither heated nor cooled during the process, and special shields for evaporation sources were used to avoid cross contamination. Glass substrates partially covered with ITO were cleaned in ultrasonic bath with isopropanol, blow-dried with hot air, and transferred into a vacuum chamber, where the following layers were subsequently evaporated: MoO₃ (5 nm), DBP (17 nm), F₁₆ZnPc (65 nm), BCP (15 nm), and Ag (50 nm). Organic materials and MoO₃ were evaporated in one vacuum cycle. The rate of evaporation of all the layers was equal to 0.2 nm/s. The active area of the samples was ca. 6 mm². The experimental setup used to collect current-voltage characteristics and short-circuit current spectra was reported in [13], while small signal admittance spectra were recorded by PM6306 FLUKE LCR meter. The root mean square voltage of 50 mV was applied in the case of all small signal measurements, while all the experiments involving illumination of the samples were run under monochromatic illumination through ITO with light of intensity $I_0 = 10^{14}$ photons/(cm²s) and either variable wavelength from the 375 nm - 900 nm range (in the case of short-circuit current action spectra) or wavelength of 600 nm.

3. Analysis and discussion

The wavelength of illumination used in all subsequent measurements was selected due to the peak value exhibited by the short-circuit current (Fig. 2a) and open-circuit voltage (Fig. 2b) action spectra within the 600 - 610 nm range, in which both active materials show high absorption (normalized absorbance of these materials, i.e. A/A_{max} where A stands for the absorbance of the layer, while A_{max} is the maximum value of this parameter recorded in the 380–900 nm range, where shown in Fig. 2a and b for the reference; values of A equal to 0.43 and 0.32 were recorded for the F₁₆ZnPc layer at $\lambda = 635$ nm and the DBP layer at $\lambda = 608$ nm, respectively). The direction of current flow and symbatic character of both action spectra (i. e. the correspondence between the maxima of current or voltage and absorption of light by active materials) within the whole investigated spectral range confirm that photovoltaic effect observed in this system is driven by exciton dissociation at the DBP/F₁₆ZnPc junction. After dissociation holes are transported through DBP to ITO, while electrons reach Ag via F₁₆ZnPc. Moreover, symbatic character of the short-circuit current action spectrum indicates that even excitons generated near the MoO₃ layer are capable of dissociation at DBP/F₁₆ZnPc interface and contribute to current flow.

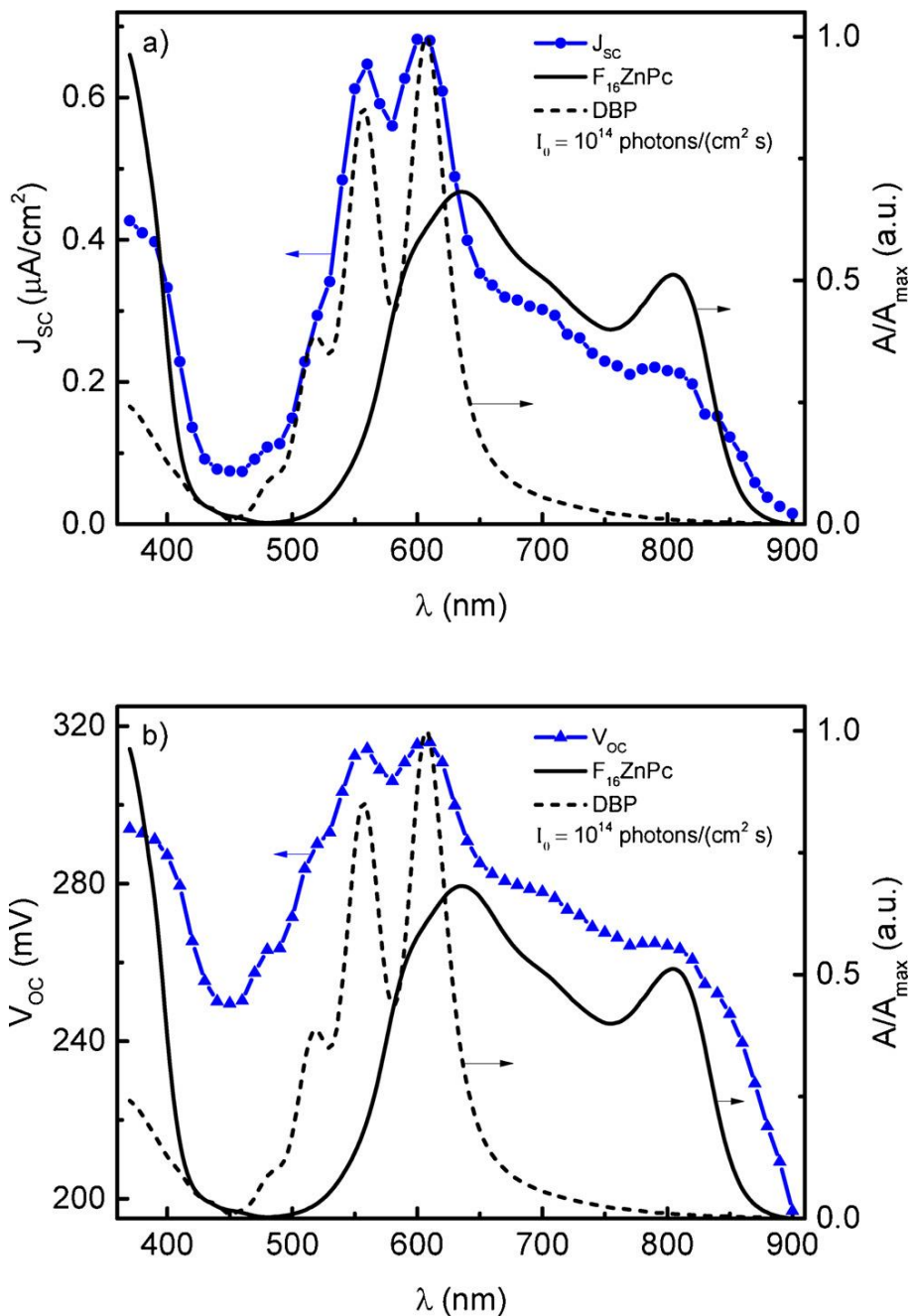


Fig. 2. Short-circuit current (a) and open-circuit voltage (b) action spectra collected for the ITO/MoO₃/DBP/F₁₆ZnPc/BCP/Ag cell illuminated through ITO with light of intensity $I_0=10^{14}$ photons/(cm²s) (blue circles and triangles), along with normalized absorbance of DBP (dashed line) and F₁₆ZnPc (solid line). Current flows from Ag to ITO.

Fig. 3 shows current-voltage characteristics collected in the dark (solid squares) and under illumination (circles). Positive voltage corresponds to higher potential at ITO. Solid circles show current flowing from ITO to Ag, while open circles correspond to current flowing from Ag to ITO. At $\lambda = 600$ nm and under such relatively low light intensity the short-circuit current reaches ca. $0.8 \mu\text{A}/\text{cm}^2$, while the open-circuit voltage yield 0.35 V. According to R. A. J. Janssen and J. Nelson [27] the offset between the hole-transporting level of DBP and the electron-transporting level of F₁₆ZnPc of 0.9 eV should be sufficient to provide the V_{oc} of about 0.6 V under higher illumination intensities. The inset of Fig. 3 shows a semi-log plot of the dark current-voltage curve that cannot be fitted to the modified diode equation characteristic for semiconductor p-n junctions, since we would observe an increase in the diode ideality factor n (extracted in the same manner as in [28]) from 1.4 at 0.1 V to 6.5 at 0.8 V, that cannot be explained within the frame of Shockley equation [29]. Such a situation is quite common for organic solar cells.

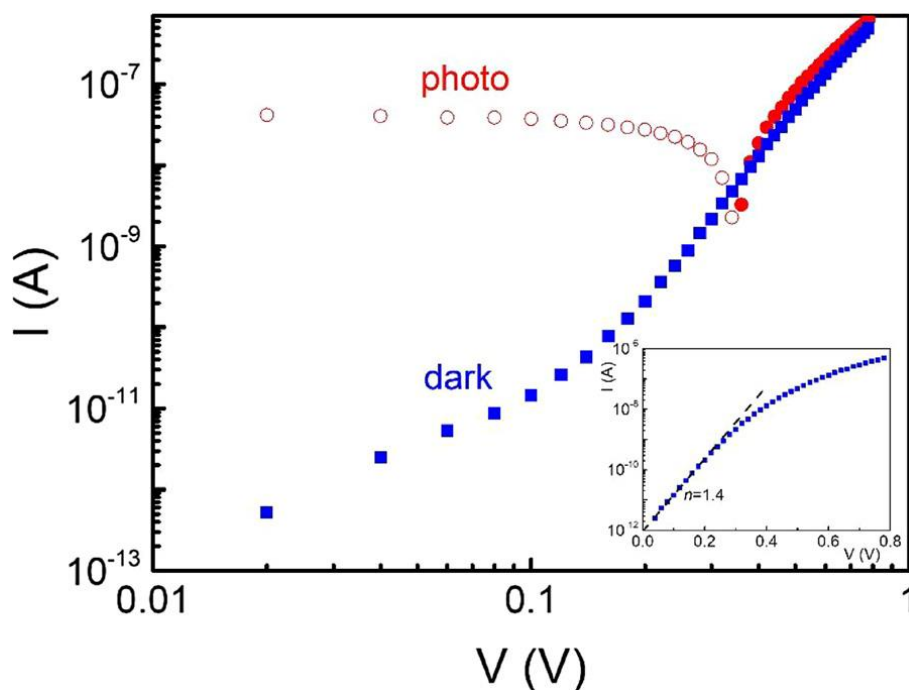


Fig. 3. Current-voltage characteristics of the ITO/MoO₃/DBP/F₁₆ZnPc/BCP/Ag system in the dark (blue squares) and under illumination with $\lambda=600$ nm and $I_0=10^{14}$ photons/(cm²s) from the ITO side (red circles). Solid and open symbols correspond to current flowing from ITO to Ag and from Ag to ITO, respectively. Inset shows the semi-log plot of the dark current, while n stands for the diode ideality factor.

Spectra of small signal conductance and capacitance collected for the investigated system in the dark and under illumination are presented in Figs. 4 and 5 respectively in the form of conductance (Y'), i.e. a real part of admittance, and the real part of capacitance (C'). Firstly, it is worth noticing that the spectrum of C' does not depend on applied steady voltage nor illumination. In this spectrum we distinguish two nF capacitances independent of frequency in a wide range of frequencies. Thus, spectrum of capacitance seems to be determined by two ideal capacitors. Situation changes in the case of conductance - for higher frequencies (just above ca. $6 \cdot 10^3$ Hz) the curves are practically independent of steady voltage, while for lower frequencies a clear effect of steady voltage is seen. Looking from lower to higher frequencies we can generally notice three steps of the curves. The lowest one depends on steady voltage and is explicitly noticeable at $V = 0.8$ V. The middle one does not depend on steady voltage and is seen at around 10 kHz. The existence of the highest step can be deduced from the continuous increase in the logarithm of conductance with logarithm of frequency observed for the frequencies above 100 kHz. Taking into account the above consideration we can propose the equivalent circuit of the investigated device consisting of 5 ideal elements, namely two capacitors and three resistors, that could be connected as shown in Fig. 6. Assuming this kind of a connection, we may easily distinguish the resistance of electrodes and a geometric capacitance. By resistance of electrodes we mean an ohmic resistance resulting mainly from the thickness of the top electrode (the issue was discussed in [30]). By geometric capacitance we, like many others (e.g [31]), mean capacitance of the system composed of regarded layers (with no free charge carriers) sandwiched between parallel electrodes. Geometric capacitance results from dielectric polarizability, so it is determined by the permittivity of sandwiched layers and their thickness. In the proposed equivalent system, R_0 could be the resistance of electrodes, while $C_1 C_2 / (C_1 + C_2)$ the geometric capacitance.

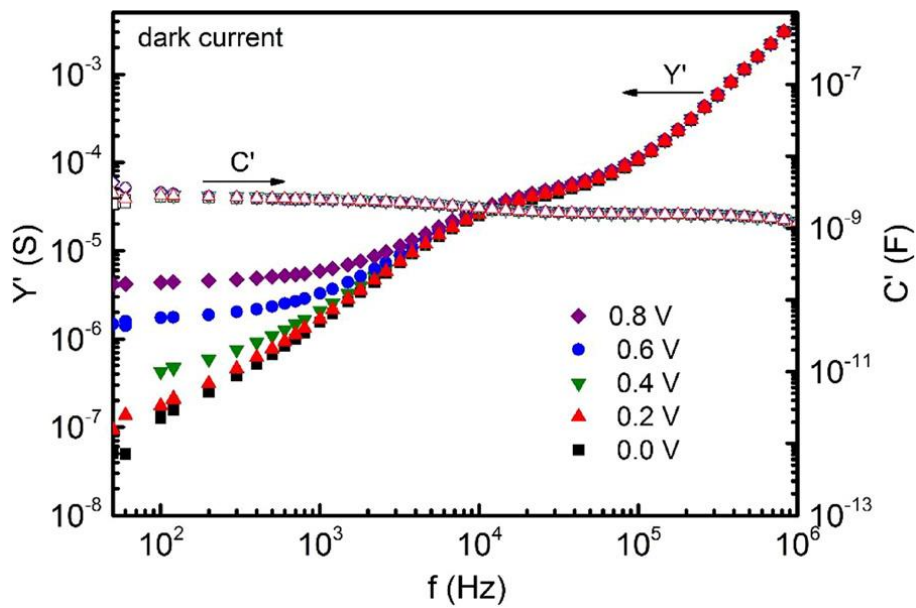


Fig. 4. Small-signal conductance (solid symbols) and capacitance (open symbols) spectra collected in the dark for various values of steady voltage at higher potential on ITO.

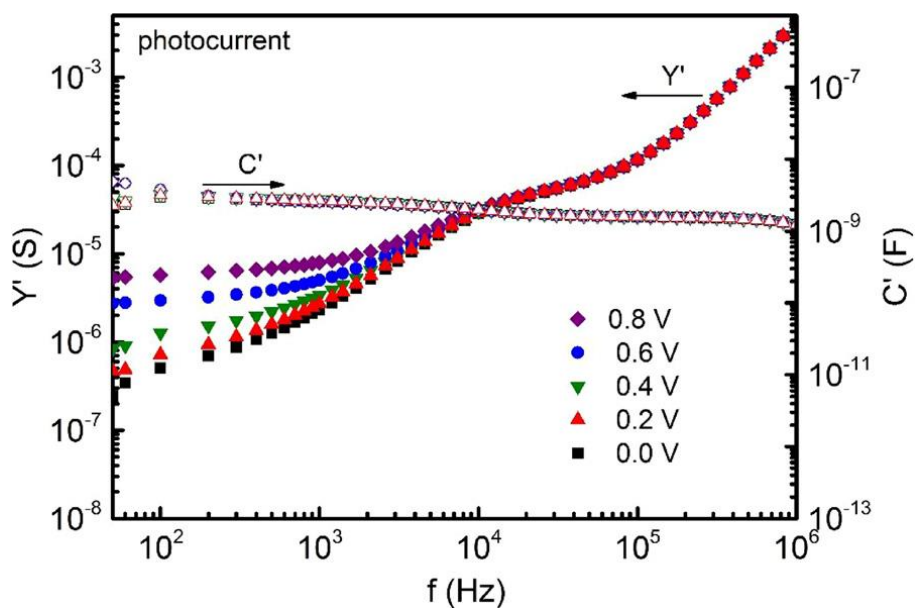


Fig. 5. Small-signal conductance (solid symbols) and capacitance (open symbols) spectra under illumination through ITO with light of wavelength of 600 nm and intensity of 10^{14} photons/(cm²s) collected for various values of steady voltage at higher potential on ITO.

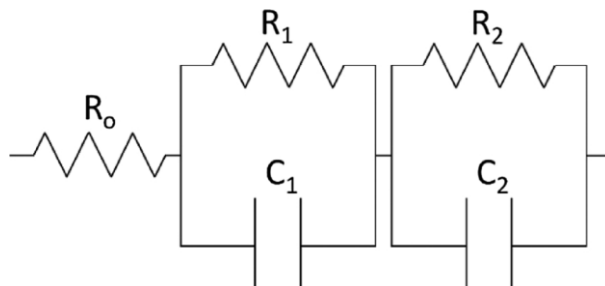


Fig. 6. Equivalent circuit proposed for interpretation of experimental results.

To verify the choice of the equivalent circuit and to evaluate the values of resistances and capacities of particular elements of that circuit we fitted the experimental results of admittance spectra (Figs. 7 and 8) with simulated curves, separately for each value of steady voltage. As it is seen, good correlation between simulated curves (lines) and experimental data (symbols) was obtained for higher values of steady voltage (for V higher than ca. 0.4 V).

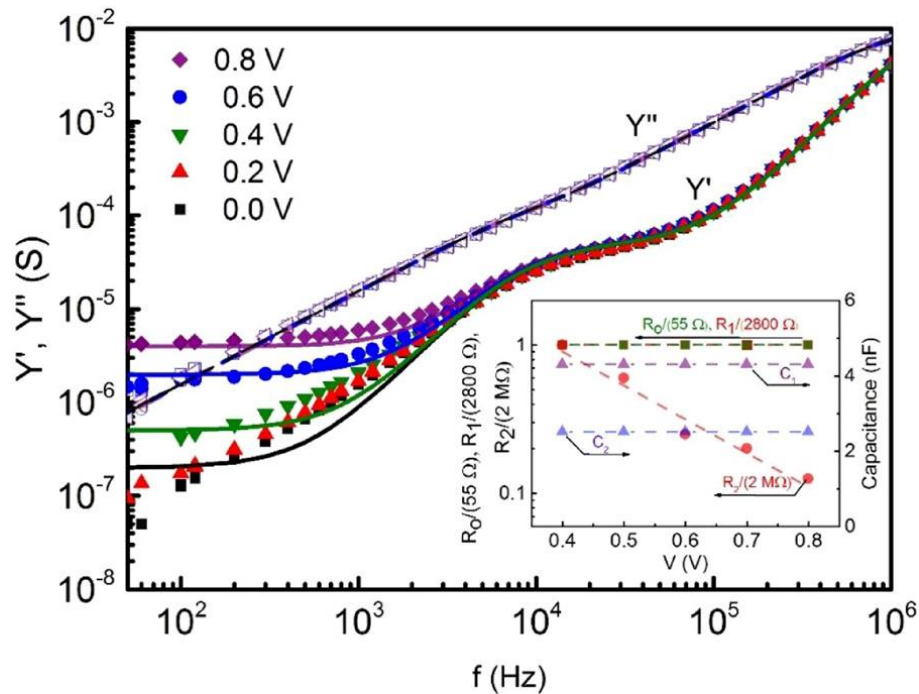


Fig. 7. Small signal conductance (Y') and susceptance (Y'') spectra obtained in the dark at selected values of steady voltage with the ITO at higher potential: symbols – experimental results, lines – simulated curves for the equivalent circuit presented in Fig. 6. Inset presents parameters of all five elements of the equivalent circuit (symbols) obtained from the best fit versus steady voltage.

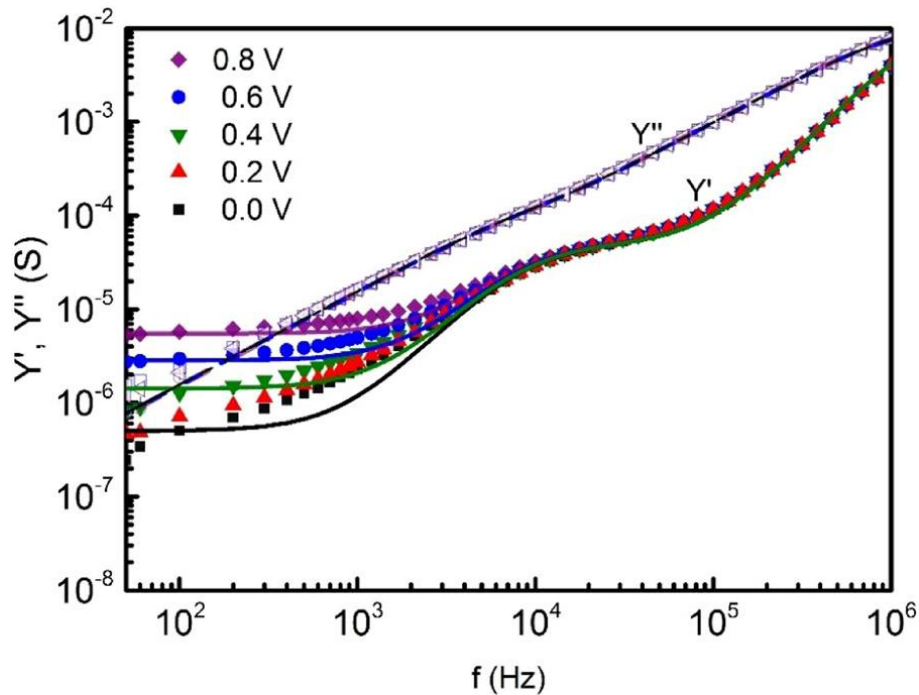


Fig. 8. Small signal conductance (Y') and susceptance (Y'') spectra under illumination with light of 600 nm and 10^{14} photons/(cm^2s) from the ITO side at selected values of steady voltage with the ITO at higher potential: symbols – experimental results, lines – simulated curves obtained for the equivalent circuit presented in Fig. 6.

The next step was to analyse the relation between low frequency conductance defined as

$$Y'_{LF} = \lim_{f \rightarrow 0} Y' \quad (1)$$

and differential direct current conductance defined as

$$G_{dc} = \frac{dI}{dV} \quad (2)$$

since for small signal admittance the following condition should be satisfied:

$$Y'_{LF} = G_{dc} \quad (3)$$

Fig. 9 shows differential direct current conductance (G_{dc} , lines) calculated from the data shown in Fig. 3, along with small signal conductance taken from experimental spectra (Figs. 7 and 8) at a frequency equal to 100 Hz (Y'_{100} , symbols). The values of these parameters are consistent with each other for higher values of steady voltage both in the dark and under illumination. On the other hand, for lower values of steady voltage the dark Y'_{100} differs from the dark G_{dc} , but the former correlates well with the G_{dc} under illumination. It is worth noticing, that within this range of steady voltage the Y'_{100} is of the same order of magnitude in the dark and under illumination (10^{-7} S and 5×10^{-7} S respectively) much greater than the dark G_{dc} . Furthermore, the Y'_{100} in the dark and under illumination is almost independent of steady voltage within the lower range of voltages. The increase in the Y'_{100} is observed for voltages higher than ca. 0.4 V, where the Y'_{100} conductance follows G_{dc} .

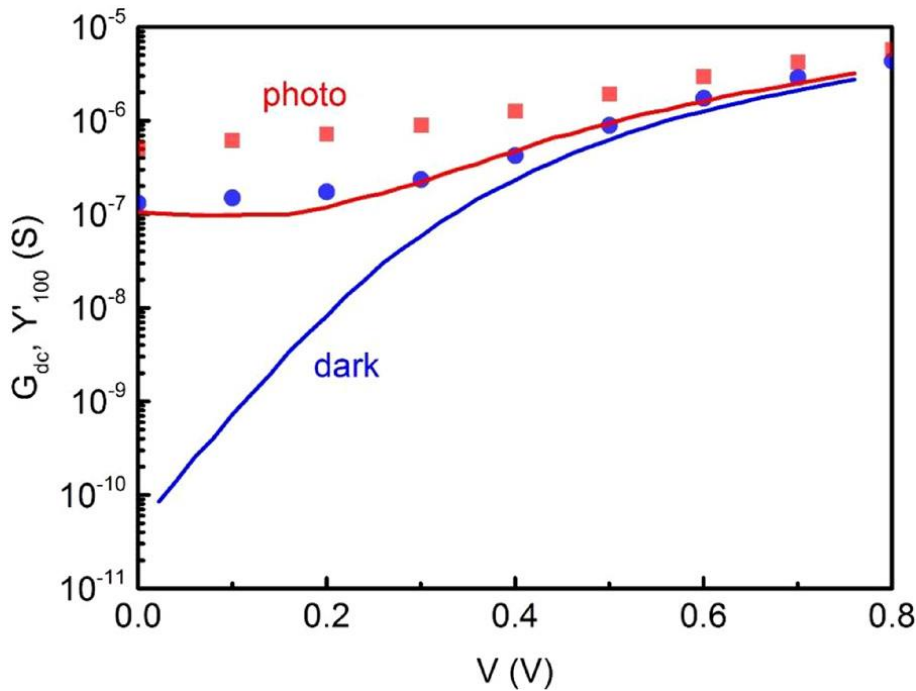


Fig. 9. Differential direct current conductance (G_{dc}) in the dark (blue line) and under illumination (red line) as well as the conductance (Y'_{100}) in the dark (blue circles) and under illumination (red squares) versus steady voltage.

Let us now take into account all properties mentioned above. Firstly, we shall consider the range of voltages where good correlation between direct current and small signal responses occurs, i. e. steady voltage > 0.4 V. Since good correlation between simulations and small signal spectra is observed in this range, and simultaneously the relation given by Eq. (3) is valid, we can say that our equivalent circuit is complete. It means that we do not need any additional elements to explain small signal spectra, or in other words, no other element can be deduced from small signal spectra even if frequencies lower than these applied herein are used. Let us now analyse the values of parameters obtained for particular elements from simulations. The inset of Fig. 7 presents these parameters as a function of steady voltage. As it is clearly seen, only one parameter, namely R_2 explicitly depends on voltage, while the others are practically constant. Such behavior can suggest that these four parameters, namely R_0 , R_1 , C_1 , C_2 , origin from geometry of the system under study. $C_1 = 4.3$ nF and $C_2 = 2.5$ nF may be attributed to geometric capacitances of DBP and $F_{16}ZnPc$ layers respectively. However, taking into account the thickness, active

area, and permittivity of each layer we would expect a bit higher values of capacitances. Therefore, we can suppose that C_1 is not a pure geometric capacitance of DBP film but it can be a geometric capacitance of DBP and MoO_3 layers connected in series. Analogically, C_2 could be regarded as a geometric capacitance of the $\text{F}_{16}\text{ZnPc}/\text{BCP}$ bilayer. Moreover, in contrast to the semiconductor p-n junctions, no effect of space charge at electron donor/electron acceptor interface is noticeable, since in the case of p-n junctions the capacitance of space charge region explicitly depends on steady voltage.

If we assume that C_1 and C_2 connected in series account for the geometric capacitance of $\text{MoO}_3/\text{DBP}/\text{F}_{16}\text{ZnPc}/\text{BCP}$ then R_0 can be regarded as the resistance of electrodes. Such resistance obviously does not depend on steady voltage and the value of 55Ω obtained for the investigated system is rather typical for the electrode resistance in organic devices [30,32–34].

To interpret R_1 and R_2 it is worth noticing that R_1 is in parallel configuration to C_1 and R_2 is in parallel configuration with C_2 (see Fig. 5). So, R_1 can be roughly related to the resistance of DBP and R_2 can be roughly related to the resistance of F_{16}ZnPc . Moreover, we see that R_1 is much lower than R_2 and independent of steady voltage. As $R_1 \ll R_2$ and the thickness of DBP layer is only twice lower than F_{16}ZnPc we can suppose that conductivity of DBP is much higher than conductivity of F_{16}ZnPc . It is not a surprising result, since generally in the case of organic materials a hole-transporting layer usually conducts electric current much better than an electron-transporting layer. Moreover, as R_1 does not depend on steady voltage we can say there is no barrier for holes entering DBP from ITO via MoO_3 . Different situation is observed for R_2 , which decreases with increasing voltage. As the current is flowing from ITO to Ag and F_{16}ZnPc is an organic material of acceptor properties, we can relate R_2 to the transport of electrons from Ag to $\text{F}_{16}\text{ZnPc}/\text{DBP}$ junction. Therefore, the effect of voltage on R_2 could result from either injection of electrons from Ag to F_{16}ZnPc via BCP or transport of electrons in F_{16}ZnPc , or recombination of electrons with holes at $\text{F}_{16}\text{ZnPc}/\text{DBP}$. In our opinion the most probable process determining voltage dependence of R_2 seems to be the first case, namely electron injection from Ag into F_{16}ZnPc . We think so, because R_2 is connected in parallel with geometric capacitance of $\text{F}_{16}\text{ZnPc}/\text{BCP}$ layers. Moreover, we would not observe a pure geometric capacitance in the case of space charge limited current, since then a time of flight modulates small-signal-capacitance spectra [35,36]. We would not observe it also in the presence of space charge at a p-n junction since in this case the measured capacitance is much higher than the geometric one and voltage-dependent [29].

Interesting situation occurs for steady voltage lower than 0.4 V. The steady dark current still seems to be determined by electron injection from Ag into F_{16}ZnPc , as G_{dc} decreases with decreasing voltage (blue line Fig. 9), however the dark Y'_{100} (blue circles) does not follow G_{dc} . The Y'_{100} stays at the level of 10^{-7} S , that is much higher than G_{dc} for the dark current. Hence, we can predict that for frequencies lower than investigated the small-signal conductance will drop to the values correlating to the dc curve. We can say that within this range of steady voltage, our equivalent circuit is not complete. Interesting is also the fact, that the level of 10^{-7} S correlates to G_{dc} of the photovoltaic curve (red line in Fig. 9). A constant level of G_{dc} within the photovoltaic range generally results from parasitic resistance and when this conductance is observed nearby the short-circuit of photovoltaic cell it usually originates from parallel parasitic resistance [37]. For our device the parallel parasitic resistance is also seen in small signal response, since the Y'_{100} both in the dark and under illumination follows G_{dc} within photovoltaic region. So we come to conclusion that under low steady bias small signal conductance in the dark and under illumination is determined by parallel parasitic resistance of our photovoltaic cell.

Let us look at experimental data at steady voltage below 0.4 V regarding that $10^7 \Omega$ is just a parallel parasitic resistance. As we mentioned previously, the presence of this resistance is noticeable in the dark small signal spectra, however the dark direct current is determined by much higher resistance that has to be connected in series to the parasitic resistance. On the other hand, this much higher resistance does not affect the photovoltaic current. We think that such behavior can be related to the direction of the current flow. The photovoltaic current flows from Ag to ITO, while the dark current flows from ITO to Ag. In the photovoltaic regime we do not see any effective resistance connected in series, so we can say that holes generated at the $\text{DBP}/\text{F}_{16}\text{ZnPc}$ junction can easily enter ITO from DBP via MoO_3 and electrons generated at the $\text{DBP}/\text{F}_{16}\text{ZnPc}$ junction can easily enter Ag from F_{16}ZnPc via BCP. In the dark there must be however a barrier for injection of either electrons from Ag via BCP to F_{16}ZnPc or holes from ITO via MoO_3 to DBP.

We think that the presence of the former barrier is more probable, since greater resistance, i.e. R_2 , is connected to C_2 in our equivalent circuit.

The statement that the injection of free charge carriers from the electrode determines the dark current flow is also supported by experimental results obtained under bias greater than 0.4 V. Namely, the increase in the current injected from electrodes at higher electric fields can account for the increase in G_{dc} over 10^{-7} S observed under this bias.

4. Conclusions

Simultaneous analysis of both components of complex admittance and their relation to direct current-voltage curves collected in the dark and under illumination proposed herein can be a valuable tool for determination of physical processes related to electric charge transport within multilayer structures, such as photovoltaic cells or photodetectors. Such an analysis may provide information on potential barriers, parasitic resistances and presence of space charge affecting the electric current flow through the device. Moreover, the analysis of small signal spectra may be applied as an easy method of evaluation of electrode resistance and of geometric capacitance of the investigated system.

Using this approach for the investigated ITO/MoO₃/DBP/F₁₆ZnPc/BCP/Ag structure, we managed to propose equivalent circuits of the investigated system, i.e. capacities, resistances and the type of their connection, and to relate these elements to physical processes taking place within this system subjected to external bias. We came to a conclusion that processes determining charge transport depend on the direction of current flow. The dark direct current-voltage curve is determined by electrode injection of free charge carriers, most probably by electron injection from Ag into F₁₆ZnPc via BCP. Nevertheless, there are no potential barriers for collection of free holes and electrons photogenerated at the donor/acceptor interface, i.e. for the extraction of holes from DBP into ITO via a thin layer of MoO₃ nor for electrons flowing from F₁₆ZnPc to Ag via a thin film of BCP.

References

- [1] M.A. Green, Y. Hishikawa, E.D. Dunlop, D.H. Levi, J. Hohl-Ebinger, A.W.Y. Ho-Baillie, *Prog. Photovolt. Res. Appl.* 26 (2018) 3.
- [2] W. Shockley, H.J. Queisser, *J. Appl. Phys.* 32 (1961) 510.
- [3] T. Kirchartz, W. Gong, S. Hawks, T. Agostinelli, R.C.I. MacKenzie, Y. Yang, J. Nelson, *J. Phys. Chem. C* 116 (2012) 7672.
- [4] S.W. Tsang, S.K. So, J.B. Xu, *J. Appl. Phys.* 99 (2006) 013706.
- [5] Y.Q. Zheng, C. Wang, J. Le Yu, F. Yang, B. Wei, Y. Lin, F. Li, Xi F. Li, C. Adachi, *Synth. Met.* 233 (2017) 35.
- [6] S. Nam, J. Seo, M. Song, H. Kim, M. Ree, Y.-S. Gal, D.D.C. Bradley, Y. Kim, *Org. Electron.* 48 (2017) 61.
- [7] M.R. Kiran, H. Ulla, M.N. Satyanarayan, G. Umesh, *Synth. Met.* 224 (2017) 63.
- [8] C.-h. Chen, A. Kine, R.D. Nelson, J.C. LaRue, *Synth. Met.* 206 (2015) 106.
- [9] T. Zhuang, T. Sano, J. Kido, *Org. Electron.* 26 (2015) 415.
- [10] D. Fujishima, H. Kanno, T. Kinoshita, E. Maruyama, M. Tanaka, M. Shirakawa, K. Shibata, *Sol. Energy Mater. Sol. Cells* 93 (2018) 20090 1029.
- [11] X. Xiao, J.D. Zimmerman, B.E. Lassiter, K.J. Bergemann, S.R. Forrest, *Appl. Phys. Lett.* 102 (2013) 073302.
- [12] Y. Peng, L. Zhang, T.L. Andrew, *Appl. Phys. Lett.* 105 (2014) 083304.
- [13] J. Szostak, R. Signerski, J. Godlewski, *Physica Status Solidi A Appl. Res.* 210 (2013) 2353.
- [14] J. Szostak, *Photovoltaic Phenomena in Devices With Perfluorozincphthalocyanine Layer*, PhD Thesis, Faculty of Applied Physics and Mathematics, Gdańsk University of Technology, Gdańsk, 2016.
- [15] S. Yoon, H. Kim, E.-Y. Shin, I.-G. Bae, B. Park, Y.-Y. Noh, I. Hwang, *Org. Electron.* 32 (2016) 200.
- [16] N. Wang, J. Yu, Y. Zang, J. Huang, Y. Jiang, *Sol. Energy Mater. Sol. Cells* 94 (2010) 263.
- [17] Y.-Q. Zheng, W.J. Potscavage Jr, J. Zhang, T. Yasuda, B. Wei, C. Adachi, *Synth. Met.* 205 (2015) 121.
- [18] S. Kalia, A. Mahajan, C.G. Ghansyam, R.K. Bedi, *J. Appl. Phys.* 121 (2017) 225501.

- [19] M. Zhang, H. Wang, H. Tian, Y. Geng, C.W. Tang, *Adv. Mater.* 23 (2011) 4960.
- [20] J.W. Ma, Z. Liang, C. Jin, X.Y. Jiang, Z.L. Zhang, *Solid State Commun.* 149 (2009) 214.
- [21] A. Hassan, B. Kadem, W. Cranton, *Thin Solid Films* 636 (2017) 760.
- [22] H. Liang, Z. Luo, R. Zhu, Y. Dong, J.-H. Lee, J. Zhou, S.-T. Wu, *J. Phys. D Appl. Phys.* 49 (2016) 145103.
- [23] M. Pfeiffer, K. Leo, N. Karl, *J. Appl. Phys.* 80 (1996) 6880.
- [24] F. Huang, Y. Peng, K. Xu, W. Lv, S. Xu, Y. Wang, Y. Tang, Y. Wei, Y. Yang, G. Liu, *J. Phys. D Appl. Phys.* 50 (2017) 205106.
- [25] Y. Zheng, F. Yang, C. Wang, J. Zhang, W.J. Potscavage Jr, B. Wei, C. Adachi, W. Pu, C. Yang, J. Zhang, *Synth. Met.* 221 (2016) 179.
- [26] H.B. Michaelson, *J. Appl. Phys.* 48 (1977) 4729.
- [27] R.A.J. Janssen, J. Nelson, *Adv. Mater.* 25 (2013) 1847.
- [28] F. Aziz, K. Sulaiman, W.K. Al-Rawi, Z. Ahmad, M.H. Sayyad, Kh.S. Karimov, L.L. Wei, M. Tahir, *Pigments Resin Technol.* 44 (2015) 148.
- [29] S.M. Sze, Kwok K. Ng, *Semiconductor Devices*, John Wiley & Sons, Inc., Hoboken, New Jersey, 2007.
- [30] G. Jarosz, R. Signerski, L. Brehmer, *Thin Solid Films* 514 (2006) 287.
- [31] P. Stallinga, *Electrical Characterization of Organic Electronic Materials and Devices*, John Wiley&Sons Ltd, United Kingdom, 2010.
- [32] L. Burtone, D. Ray, K. Leo, M. Riede, *J. Appl. Phys.* 111 (2012) 064503.
- [33] C.-H. Lin, S.-C. Tseng, Y.-K. Liu, Y. Tai, S. Chattopadhyay, C.-F. Lin, J.-H. Lee, J.-S. Hwang, Y.-Y. Hsu, Li-C. Chen, W.-C. Chen, K.-H. Chen, *Appl. Phys. Lett.* 92 (2008) 233302.
- [34] X.W. Zhang, J.-W. Xu, H.-R. Xu, H. Wang, L.C. Xie, B. Wei, X.-Y. Jiang, Z.-L. Zhang, *J. Phys. D Appl. Phys.* 46 (2013) 055102.
- [35] J. Shao, G.T. Wright, *Solid State Electron.* 3 (1961) 291.
- [36] G. Jarosz, R. Signerski, *Synth. Met.* 179 (2013) 49.
- [37] P. Würfel, *Physics of Solar Cells*, WILEY-VCH Verlag GmbH&Co., KGaA, Weinheim, 2005.

